

Article

A Holistic View of the Interactions between Electron-Deficient Systems: Clustering of Beryllium and Magnesium Hydrides and Halides

Otilia Mó ^{1,*}, M. Merced Montero-Campillo ^{1,*}, Manuel Yáñez ¹, Ibon Alkorta ^{2,*} and José Elguero ²

¹ Departamento de Química, Módulo 13, Facultad de Ciencias, and Institute of Advanced Chemical Sciences (IAdChem), Universidad Autónoma de Madrid, Campus de Excelencia UAM-CSIC, Cantoblanco, 28049 Madrid, Spain; otília.mo@uam.es (O.M.); manuel.yanez@uam.es (M.Y.)

² Instituto de Química Médica, IQM-CSIC, Juan de la Cierva, 3, 28006 Madrid, Spain; iqmbe17@iqm.csic.es

* Correspondence: mm.montero@uam.es (M.M.M.-C.); ibon@iqm.csic.es (I.A.); Tel.: +34-91-497-3462 (M.M.M.-C.); +34-91-258-706-75 (I.A.)

Abstract: In the search for common bonding patterns in pure and mixed clusters of beryllium and magnesium derivatives, the most stable dimers and trimers involving BeX₂ and MgX₂ (X = H, F, Cl) have been studied in the gas phase using B3LYP and M06-2X DFT methods and the G4 ab initio composite procedure. To obtain some insight into their structure, stability, and bonding characteristics, we have used two different energy decomposition formalisms, namely MBIE and LMO-EDA, in parallel with the analysis of the electron density with the help of QTAIM, ELF, NCIPLOT, and AdNDP approaches. Some interesting differences are already observed in the dimers, where the stability sequence observed for the hydrides differs entirely from that of the fluorides and chlorides. Trimers also show some peculiarities associated with the presence of compact trigonal cyclic structures that compete in stability with the more conventional hexagonal and linear forms. As observed for dimers, the stability of the trimers changes significantly from hydrides to fluorides or chlorides. Although some of these clusters were previously explored in the literature, the novelty of this work is to provide a holistic approach to the entire series of compounds by using chemical bonding tools, allowing us to understand the stability trends in detail and providing insights for a significant number of new, unexplored structures.

Keywords: Be and Mg hydrides and halides; clusters; bonding; rehybridization; stability trends; multicenter bond



Citation: Mó, O.; Montero-Campillo, M.M.; Yáñez, M.; Alkorta, I.; Elguero, J. A Holistic View of the Interactions between Electron-Deficient Systems: Clustering of Beryllium and Magnesium Hydrides and Halides. *Molecules* **2023**, *28*, 7507. <https://doi.org/10.3390/molecules28227507>

Academic Editor: Wim Buijs

Received: 3 October 2023

Revised: 24 October 2023

Accepted: 27 October 2023

Published: 9 November 2023



Copyright: © 2023 by the authors. Licensee MDPI, Basel, Switzerland. This article is an open access article distributed under the terms and conditions of the Creative Commons Attribution (CC BY) license (<https://creativecommons.org/licenses/by/4.0/>).

1. Introduction

Electron-deficient compounds very often exhibit peculiar bonding characteristics. The most paradigmatic example is diborane, in which the two BH₃ monomers share two hydrogen atoms. As a result of the formation of this quite singular bond, three centers share a pair of electrons as in any typical two-center covalent bond [1,2]. These bonding arrangements, usually named three-center two-electron (3c-2e) bonds, are also found in dialane, the corresponding aluminum hydride dimer. On top of these singular bonding patterns, electron-deficient compounds often present elusive aggregates. A typical example is the corresponding aluminum hydride, whose dimer was predicted to be stable by ab initio calculations [3,4] in the late 1980s but would not be characterized experimentally for the first time until the beginning of the XXI century [5]. In contrast to the stability of diborane, diborane halides, namely B₂F₆ and B₂Cl₆, which were supposedly not stable in the gas phase [6], were very recently found to be weakly bound, as revealed by high-level ab initio calculations. The low stabilization enthalpies are due to the fact that interaction between monomers is mainly dispersion [7]. In the same paper, a systematic study of dimers and trimers involving BX₃ and AlX₃ (X = H, F, Cl) in the gas phase showed that

besides dispersion, the rehybridization of the electron-deficient element and its ability to reach pentacoordination are key factors to understand their structure, stability, and bonding characteristics. These findings prompted us to explore the behavior of similar dimers and trimers involving electron-deficient elements from group IIA of the periodic table. Accordingly, in the present paper, we present a theoretical examination of dimers and trimers involving BeX_2 and MgX_2 ($X = \text{H}, \text{F}, \text{Cl}$) in the gas phase.

Not surprisingly, BeH_2 and its dimer have received a lot of attention. The first two studies we are aware of were on Be_2H_4 and Be_3H_6 [8] at the Hartree–Fock level, with an estimation of electron correlation effects, and on Be_2H_4 and Mg_2H_4 using non-empirical approaches, the latter one including also the mixed BeMgH_4 dimer [9]. A rather complete survey of the dimers, trimers, and tetramers of BeH_2 and MgH_2 using high-level ab initio calculations was published in 2005 [10]. More recently, an analysis of the properties of Be_2H_4 and other beryllium hydride oligomers and their spectral characteristics have been reported [11], but the Be_3H_6 trimer was not included in this survey [11]. In 2011, a study of the interactions of BeH_2 and Mg_2H_4 with H_2 included information on the structure and energetics of these two clusters, revealing their ability for hydrogen storage purposes [12]. The Raman spectrum of Be_2H_4 (D_{2h}) was predicted [13] using a new code from variational configuration interaction theory to allow the calculation of such spectra in a pure ab initio fashion [14]. The magnesium hydride dimer was characterized by matrix infrared spectroscopy, which led to the conclusion that Mg_2H_4 is a dibridged molecule analogous to dialane [15]. Some attention was also paid to polymers of BeH_2 [16,17]. The information is scarcer for the BeF_2 , MgF_2 , BeCl_2 , and MgCl_2 dimers. It can be reduced to Hartree–Fock calculations on Be_2F_4 , Mg_2F_4 , and BeF_2MgF_2 clusters [18], calculations based on polarized models for MgF_2 and MgCl_2 [19], SCF calculations on the dimers of BeF_2 , BeCl_2 , MgF_2 , and MgCl_2 [20], and electron diffraction experiments on the MgCl_2 dimer [21]. For the specific case of the BeCl_2 dimer, gas-phase electron diffraction (GED) and mass spectrometric (MS) experiments allowed us to obtain its structure assuming a D_{2h} symmetry, and its force constants and frequencies were also estimated [22]. Some complexes involving Be_2Cl_4 and phosphorus-containing compounds have been very recently synthesized and structurally characterized, evidencing the Lewis acid behavior of beryllium in the dimer [23]. However, we are not aware of theoretical studies on trimers involving BeX_2 ($X = \text{H}, \text{F}, \text{Cl}$) derivatives, with the only exception of the BeH_2 trimer from [8,10]. The magnesium fluorides and chlorides have instead received most of the attention. To our knowledge, the first survey on the structure and energetics of $(\text{MgF}_2)_n$ clusters up to $n = 24$ was published in 1995 [24]. Years later, the structure of MgF_2 clusters, from dimers to decamers, was studied [25] using a stochastic optimization technique, namely a genetic algorithm (GA) in association with density functional theory. The structures of Mg_3Cl_6 clusters, optimized at the MP2/6-311G* level, were reported in a paper that presents a systematic study of 168 isomers of $(\text{MgCl}_2)_n$, where $n = 1\text{--}4$ [26]. It is worth noting that, with the exception of the BeMgH_4 [9] and BeMgF_4 [18] dimers, there is no information on mixed dimers or trimers involving BeX_2 and MgX_2 ($X = \text{H}, \text{F}, \text{Cl}$) compounds. The aim of this paper is to present a systematic theoretical study not only of the corresponding homodimers and homotrimers but also of the mixed dimers and trimers. Although, as indicated above, previous studies have been reported for some of these systems, most of them were focused exclusively on structures and energetics. In our study, we will focus our attention on the bonding characteristics of these clusters to precisely explain their structures and relative stabilities. We wonder what changes are observed in the bonding of the dimers when the two metals involved are not identical and how the nature of the substituent may affect bonding and relative stability trends. A similar scenario arises when dealing with trimers. What are the effects on bonding and stability when the dimer interacts with a monomer of the same nature as those forming the dimer? What occurs if the third component is a monomer different from those forming the dimer? How do these effects depend on the nature of the substituent? These are typical questions we will try to answer in this publication.

2. Results and Discussion

Since we are using high-level ab initio calculations and DFT approaches, we first compare the stabilization energies obtained with both methods. The correlation between the G4 and M06-2X values is very good (see Figure S1 of the Supplementary Materials), whereas the correlation with B3LYP functional results is worse (see Figure S2 of the Supplementary Materials). It should be noted that when dispersion contributions are included in our B3LYP calculations using the D3BJ empirical dispersion term, the total stabilization enthalpy becomes more negative from 8 to 20 kJ·mol^{−1}, improving the agreement with the G4 outcomes. However, the effects of including dispersion on the geometry of the cluster are negligibly small, to the point that if the B3LYP + D3BJ geometry is used in the standard G4 formalism (that does not include dispersion corrections in the geometry optimization procedure), the changes in the final G4 energy are typically smaller than 0.4 kJ·mol^{−1}. Hence, the conclusion is that the G4 formalism is reliable for investigating this type of complexes, in contrast to the results obtained when dealing with B and/or Al derivatives, where the dispersion effects in some of the complexes are a key factor for a proper description [7]. Additionally, in a few cases that will be commented on later, the G4 formalism predicts stationary points that, if obtained, including dispersion corrections, would collapse to the global minimum. In view of this, for the sake of simplicity, we decided to make our discussion using the M06-2X calculated values, knowing that the general conclusions are fully in line with the G4 values. All investigated clusters are closed-shell systems with stable wavefunctions.

2.1. Dimers

Standard graphical programs visualize the clusters under investigation with bonding connections based on default internuclear distances, which may lead to an ambiguous description of the systems depending on the software used. Therefore, instead, we will use the molecular graphs of the clusters in all figures in such a way that we can simultaneously have information on the shape and networking of bonds stabilizing the clusters. Following this univocal criterion, we summarized our results for the dimers in Figure 1.

Quite unexpectedly, we found that the stabilization enthalpies of the hydrides are practically equal for the three dimers, both the homodimers containing Be and Mg and the heterodimer. This is not the case, however, for the corresponding halides, in which the magnesium homodimers are clearly more stable than the beryllium homodimers and the heterodimers. It can also be observed that the largest stabilization enthalpies are those of the fluorides, being those of the chlorides not very different from those of the hydrides. Another very interesting result is that, independently of the nature of the substituent, the stabilization enthalpy of the heterodimers is very close (for the chlorides equal) to the average of the stabilization enthalpies of the corresponding homodimers. The latter observation was already suggested by Kirillov et al. for the dimer hydrides [9].

The rationalization of these findings required a detailed analysis of the bonding of these clusters. The first question we want to address is the nature of the bonds in these clusters and how they depend on the substituents. To quantify these two questions, we have carried out an LMO-EDA analysis whose results are shown in Table S1 of the Supplementary Materials. The first conspicuous fact is that the ionic character of the bonds is significant already in the hydrides, where the percentages of electrostatic and exchange components are similar, the former being slightly higher than the latter. For fluorides, the electrostatic component becomes dominant, while for chlorides, the situation is again similar to that of hydrides. This finding is fully consistent with the values of the Laplacian of the electron density, which is, in all cases, positive. However, whereas for the hydrides, the values are rather small and slightly larger for the chlorides, for fluorides, the values are from 3 to 6 times larger. The same trends are observed for the corresponding energy density values (see Figure S3 of the Supplementary Materials). The larger electrostatic weight in the fluorides is consistent with the much larger natural positive charge of Be and Mg when bonded to F and Cl (+1.7 and +1.8) with respect to the ones in the hydrides (+1.1

and +1.2). Even though the charges are similar for fluorides and chlorides, the weight of the electrostatic component is smaller in the latter due to the larger size of the substituent, which results in longer bond lengths. Another important difference between hydrides and halides, which is related to the higher covalent character of the bonds of the former, is that the three hydride dimers are stabilized by the formation of 3c-2e bonds. These bonds are not present in the halides due to the dominant electrostatic character of the interaction, as illustrated by the AdNDP analysis shown in Table S2 of the Supplementary Materials.

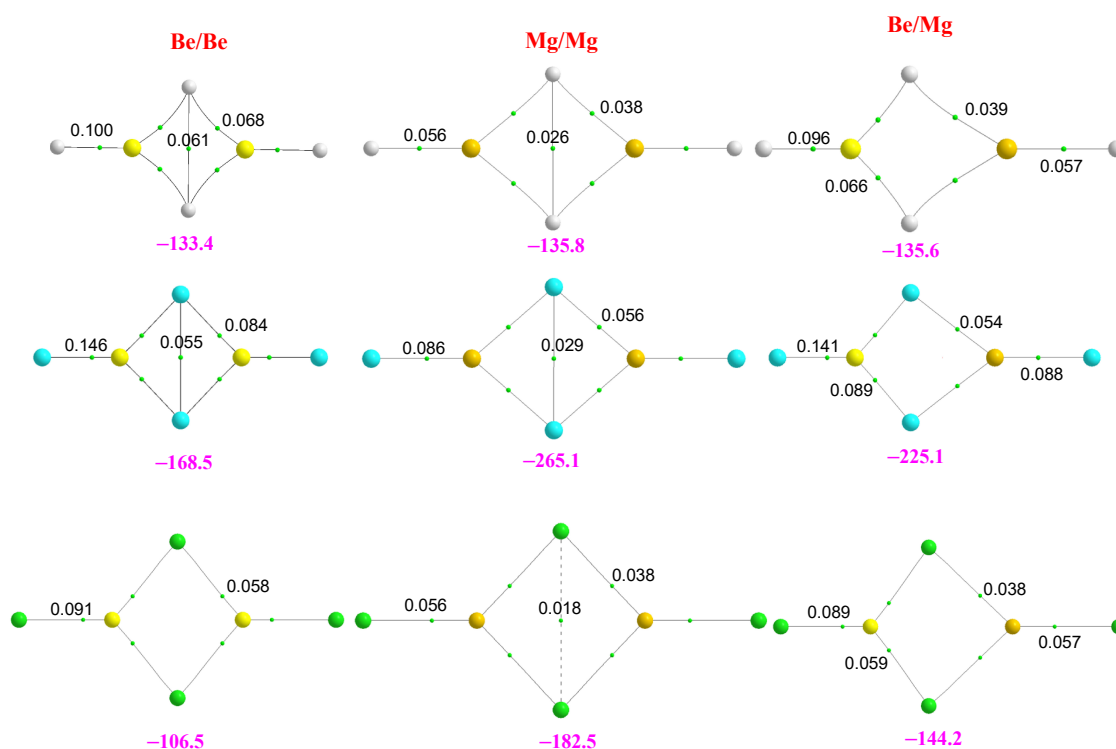


Figure 1. Molecular graphs of the homo and heterodimers involving BeX_2 and MgX_2 ($\text{X} = \text{H}, \text{F}, \text{Cl}$) monomers. The electron densities at the bond critical points (BCPs) are in a.u. The numbers in magenta are the stabilization enthalpies in $\text{kJ}\cdot\text{mol}^{-1}$. Atomic colors code: Be (yellow), Mg (orange), H (white), F (blue), Cl (green).

This result is consistent with the ELF plots (see Figure 2). It can be seen that the hydrides present trisynaptic Be-H-Be, Mg-H-Mg, and Be-H-Mg basins with a population of two electrons. In contrast, only disynaptic ones are found for fluorides, reflecting the polarization of the lone pairs of fluorine by the positive charge of the metal. The same is found for chlorides, though the polarization of the chlorine lone pairs is clearly larger, as well as the corresponding populations.

It is also worth noting that, as shown in Table 1, the dispersion contributions in these systems are not negligible, accounting for 6 to 9% of the total stabilization energy, explaining why the B3LYP+D3BJ energies are 9 to 20 $\text{kJ}\cdot\text{mol}^{-1}$ lower than the B3LYP ones.

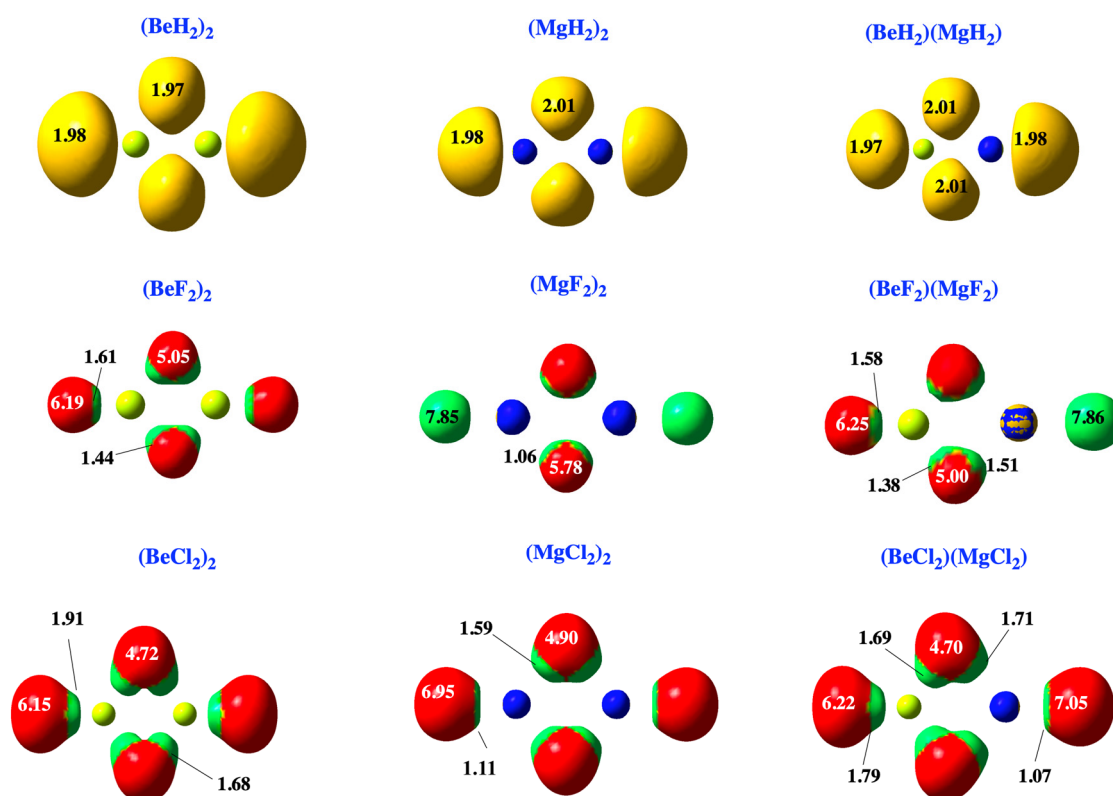


Figure 2. ELF (0.8) disynaptic and trisynaptic basins for the hydride, fluoride, and chloride homodimers and heterodimers. Basins involving H atoms are colored in yellow, and core basins involving Mg appear in dark blue. For the halides, disynaptic basins between the metal atom and fluorine atom appear in green, while lone pairs belonging to halogen atoms are colored in red. Populations are shown in atomic units (e).

Table 1. MBIE analysis of the binary complexes formed by BeX_2 and MgX_2 ($\text{X} = \text{H}, \text{F}, \text{Cl}$). All values in $\text{kJ}\cdot\text{mol}^{-1}$.

Binary Complex	$E_R(A)$	$E_R(B)$	$\Delta^2 E(AB)$	E_{total}
<i>Hydrides</i>				
BeBeH_4	58.7	58.7	−261.4	−144.1
MgMgH_4	36.3	36.3	−216.6	−143.9
BeMgH_4	66.3	31.6	−243.2	−45.2
<i>Fluorides</i>				
BeBeF_4	84.1	84.1	−340.8	−172.6
MgMgF_4	42.3	42.3	−353.1	−268.5
BeMgF_4	85.8	42.6	−357.5	−229.1
<i>Chlorides</i>				
BeBeCl_4	80.5	80.5	−269.8	−108.9
MgMgCl_4	44.2	44.2	−273.6	−185.3
BeMgCl_4	88.0	40.0	−274.8	−146.8

The stability trends within each dimer family still remain to be explained. For this purpose, it is very useful to carry out a MBIE energy decomposition analysis, which is shown in Table 1.

Starting from the hydrides, it is clear that although the stabilization energies E_{total} are practically equal for the three dimers, the stabilizing two-center energy contributions, $\Delta^2E(AB)$, are not, being the largest one that of the BeBeH₄ binary complex. In contrast, the monomer distortion E_R in the BeBeH₄ cluster is almost twice that of MgMgH₄. Indeed, the largest contribution to this term comes from the rehybridization undergone by the metal from sp to sp^n ($n \approx 2$), but this energy cost is much larger for BeH₂ than for MgH₂ (80 vs. 50 kJ·mol^{−1}) [27]. Therefore, although the attractive two-center term is larger for Be₂H₄, the larger monomer deformation energy compensates for the difference. The rehybridization cost also explains the trends for the halides. In this case, the attractive two-center contributions are rather similar, reflecting the electrostatic character of the interaction, but again, the rehybridization cost is much higher for BeF₂ than for MgF₂. Accordingly, the stabilization energy of the MgMgF₄ cluster is larger than that of the BeBeF₄ analog. Similar arguments explain the trends for the chlorides.

Finally, the stabilization enthalpy of the mixed dimers is very close to the mean of the enthalpies of the two homodimers, reflecting that the intrinsic characteristics of each monomer are essentially conserved in the dimer. This is corroborated by the different analyses. The AIM shows that the electron density at the BCP of the BeX₂ subunit practically does not change when going from the BeX₂-BeX₂ dimer to the BeX₂-MgX₂ one, and the same can be said as far as the MgX₂ subunit is concerned. The same conclusion is reached when looking at the characteristics and populations of the ELF basins, the components of the MBIE decomposition analysis, or the Wiberg bond indexes [28] (see Table S3 of the Supplementary Materials).

2.2. Homotrimers

The two most stable trimers of BeH₂ are shown in the first row of Figure 3. The most stable one corresponds to a linear aggregate, whereas the second is a cyclic structure labeled A.

Both ternary clusters can be seen as the result of the attachment of a BeH₂ monomer to the Be₂H₄ dimer, in the first case along the Be-Be axis and in the second case perpendicular to it. Accordingly, they present a very different bonding pattern, though the energy gap between them is rather small (9 kJ·mol^{−1}). This is the result, as we will discuss below, of subtle differences between the different energy components. If the stabilization enthalpy of the dimer (see Figure 1) is compared with those of the two trimers (see Figure 3), it is evident that the trimerization is followed by some kind of cooperativity since both trimers' stabilization energies are more than twice the stabilization energy of the dimer. As shown in Figure 3, the central Be atom is tetracoordinated, and according to both the AdNDP and ELF analyses, it is involved in two Be-H-Be bonds with each of the terminal Be atoms. Note, however, that the electron densities at the corresponding BCPs are greater than in the dimer, indicating stronger bonding interactions. Consistently, the ELF analysis finds trisynaptic basins in the trimer, similar to those in the dimer (see second row of Figure 3). These trisynaptic basins also have a population very close to 2 e but within a smaller volume (122 vs. 129 au³), whereas the volume of the disynaptic Be-H basins of both terminal groups remains unchanged. This contraction of the trisynaptic basins in the trimer is reflected in a shortening (0.03 Å) of the distance between the central Be atom and the terminal ones with respect to the dimer, reflecting a reinforcement of the interaction. This is also coherent with the MBIE partition energy shown in Table 2 compared to that in Table 1. The distortion energy of the terminal Be atoms are equal in the dimer and the trimer, whereas that of the central Be atom becomes about 40 kJ·mol^{−1} greater as beryllium undergoes a change of hybridization from sp^2 to sp^3 to become tetracoordinated. Consistently, the two-center contributions in the trimer are almost identical to those in the dimer, but the additional three-center term leads to its enhanced stabilization.

Table 2. MBIE analysis of the homotrimers formed by BeX₂ and MgX₂ (X = H, F). All values in kJ·mol^{−1}.

Ternary Complex	$E_R(A)$	$E_R(B)$	$E_R(C)$	$\Delta^2E(AB)$	$\Delta^2E(AC)$	$\Delta^2E(BC)$	$\Delta^3E(ABC)$	E_{total}
BeBeBeH ₆ (linear)	59.2	102.6	59.2	−262.0	7.8	−262.0	−30.9	−326.2
BeBeBeH ₆ (cyclic, A)	87.4	8.0	86.7	−202.1	−115.3	−116.0	−66.8	−318.1
BeBeBeH ₆ (hexagonal)	82.9	82.9	82.9	−140.1	−140.1	−140.1	−57.0	−228.7
MgMgMgH ₆ (linear)	37.2	66.8	37.2	−215.2	0.3	−215.2	−10.4	−299.3
MgMgMgH ₆ (cyclic, A)	58.4	4.2	58.2	−185.5	−99.6	−99.9	−30.6	−294.8
MgMgMgH ₆ (cyclic, B)	28.1	44.5	54.7	−124.6	−54.0	−188.6	−42.0	−281.9
MgMgMgH ₆ (hexagonal)	42.9	42.9	42.9	−100.1	−100.1	−100.1	−99.8	−271.4
MgMgMgH ₆ (hexagonal, non-planar)	51.6	46.7	28.5	−177.8	−77.2	−67.8	−69.3	−265.3
BeBeBeF ₆ (linear)	84.0	167.3	84.0	−345.2	−2.1	−345.2	−2.0	−359.3
BeBeBeF ₆ (hexagonal)	95.1	95.1	95.1	−175.1	−175.1	−175.1	−114.4	−354.4
BeBeBeF ₆ (cyclic, A)	162.2	29.1	162.4	−358.3	−146.2	−146.5	80.1	−217.3
BeBeBeF ₆ (cyclic, B)	78.2	124.8	181.4	−139.7	−168.9	−338.5	−40.3	−303.0
MgMgMgF ₆ (linear)	42.4	82.1	42.5	−356.3	0.3	−356.3	1.2	−546.1
MgMgMgF ₆ (cyclic, A)	92.3	16.0	92.4	−351.9	−214.4	−214.4	48.2	−531.6
MgMgMgF ₆ (cyclic, B)	39.5	56.2	63.1	−250.2	−133.0	−307.4	6.8	−525.0
MgMgMgF ₆ (hexagonal)	47.5	47.6	47.6	−188.5	−188.5	−188.5	−65.8	−488.8

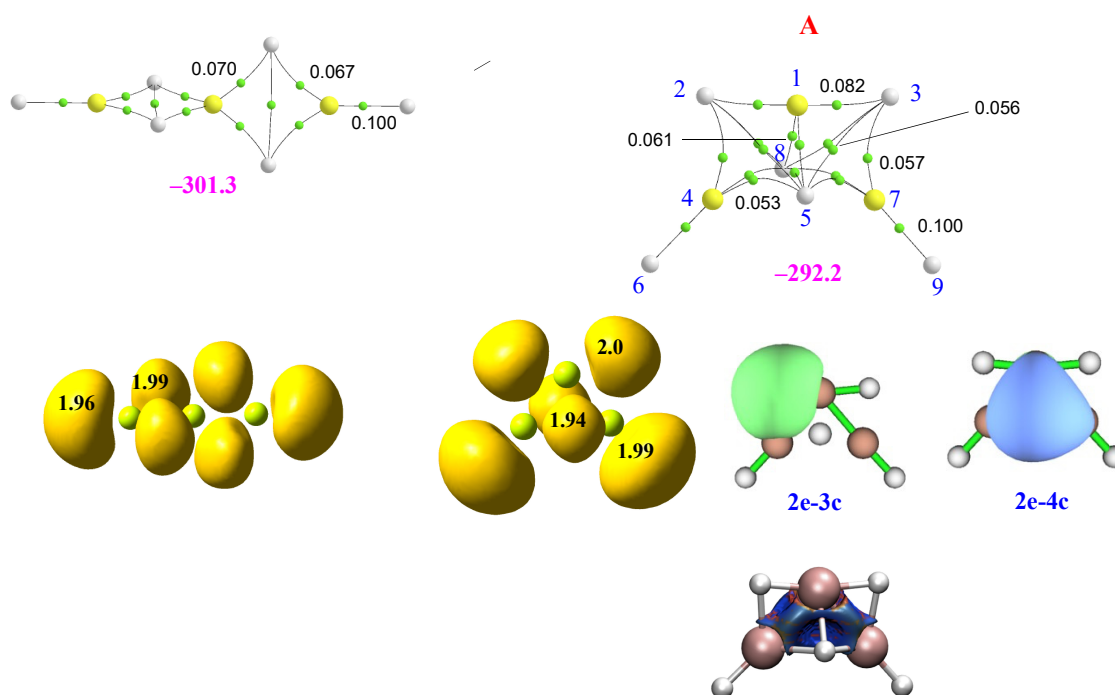


Figure 3. Molecular graphs and ELF plots of the homotrimers involving BeH_2 . The electron densities at the bond critical points (BCPs) are in a.u. The numbers in magenta are the stabilization enthalpies in $\text{kJ}\cdot\text{mol}^{-1}$. The second row shows the ELF (0.8) trisynaptic basins and their populations, as well as the 3c-2e and 4c-2e orbitals involved in the bonding of cycle **A** obtained by means of the AdNPD approach. In the third row, the 3D representation of non-covalent interactions obtained with NCIPLOT ($s = 0.3$); color code: red (strongly repulsive), green (weakly attractive and weakly repulsive), blue (strongly attractive). A less stable hexagonal trimer (not shown in the figure) is also a local minimum of the potential energy surface.

The bonding pattern of the cyclic minimum **A** is rather different. In this case, the three Be bonds are tetracoordinated, and non-covalent $\text{H}\cdots\text{H}$ interactions between the negatively charged hydrogens are also detected. The presence of these interactions implies a certain increase in the dispersion contributions to the stabilization energy, which in the cyclic trimer are significantly larger ($-198 \text{ kJ}\cdot\text{mol}^{-1}$) than in the linear cluster ($-148 \text{ kJ}\cdot\text{mol}^{-1}$). NCIPLOT shows (see third row of Figure 3) that, due to these non-covalent interactions, there is a strongly attractive and quite homogeneous interstitial density between the metals and the hydrogens, in line with the concentration of BCPs found in this area when using AIM. It can also be observed that the dimer subunit is, in this case, significantly distorted, with curved Be-H-Be bond paths, whereas the distortion of the third BeH_2 subunit is very small, with an almost linear arrangement. This subunit also appears connected to the dimer through the hydrogen atoms of the former. The AdNPD description provides some interesting additional information, showing that the connectivity between 1Be (see numbering in Figure 3) and the dimer subunit takes place through 1Be-2H-4Be and 1Be-3H-7Be 3c-2e bonds and through 1Be-5H-7Be-8H and 1Be-4Be-5H-8H 4c-2e bonds (both kinds depicted in the second row of Figure 3). The ELF description is not strictly identical since all the basins are trisynaptic, though the ones involving 4Be-5(8)H-7Be are more compact (volume 97.5 au^3) than those involving 1Be-2H-4Be and 1Be-3H-7Be (volume 141.4 au^3). The MBIE decomposition analysis shows (see Table 2) that the two-center term between the Be atoms of the dimer subunit is smaller in absolute value than in the linear trimer (-202.1 vs. $-262.0 \text{ kJ}\cdot\text{mol}^{-1}$), but the interaction of these two Be atoms with the third Be atom is more than double in cycle **A** (-66.8 vs. $-30.9 \text{ kJ}\cdot\text{mol}^{-1}$), reflecting the formation of the aforementioned 3c-2e bonds. Still, the overall attractive components in **A** are $47 \text{ kJ}\cdot\text{mol}^{-1}$

above the linear ones. Nevertheless, this difference reduces to only $9 \text{ kJ}\cdot\text{mol}^{-1}$ in the stabilization energy due to the E_R deformation energies. Indeed, the E_R distortion values of the dimer subunit of cluster **A** are higher than in the same subunits of the linear complex ($87 \text{ vs. } \text{kJ}\cdot\text{mol}^{-1}$). In contrast, the E_R value for the 1Be is much smaller ($8 \text{ kJ}\cdot\text{mol}^{-1}$) than that of the central Be atom of the linear trimer ($102 \text{ kJ}\cdot\text{mol}^{-1}$). Accordingly, the overall destabilization energies in the linear isomer are $38 \text{ kJ}\cdot\text{mol}^{-1}$ greater than in the cyclic one, reducing the gap between their stabilization energies in this amount.

The two main conclusions are that (a) it is not enough to look at the strength of the binding interactions but also at the cost of distortion they entail, and (b) the presence of weak non-covalent interactions indicates that a good description of the geometries of these cyclic clusters requires to account for dispersion, which is not contemplated in the geometry optimization of the standard G4 formalism.

For the MgH_2 trimers, the scenario, as illustrated in Figure 4, is a little more complicated, with five (only four shown in the figure) low-energy conformers instead of two. Note that the linear structure is still the global minimum.

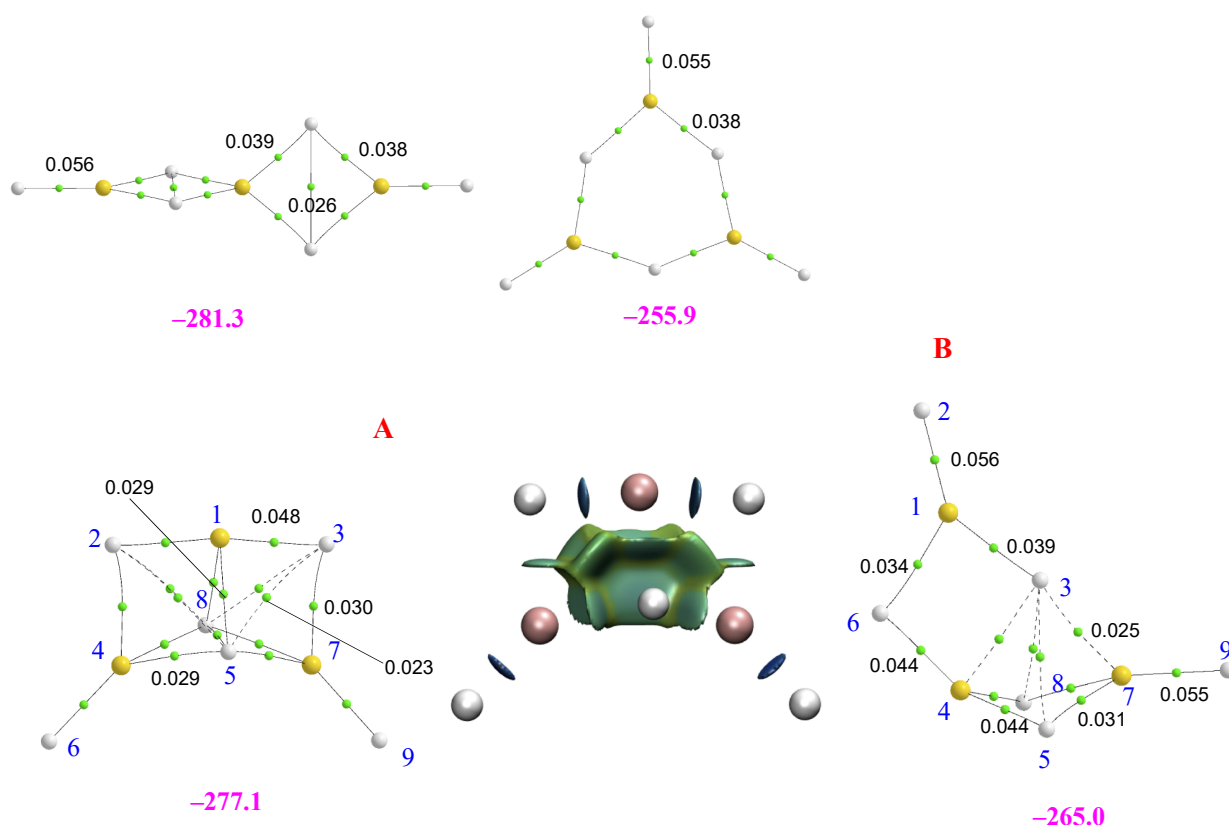


Figure 4. Molecular graphs of the homotrimers involving MgH_2 . The electron densities at the bond critical points (BCPs) are in a.u. The numbers in magenta are the stabilization enthalpies in $\text{kJ}\cdot\text{mol}^{-1}$. For cluster **A**, the 3D representation of non-covalent interactions obtained with NCIPLOT ($s = 0.3$); color code: red (strongly repulsive), green (weakly attractive and weakly repulsive), blue (strongly attractive), is included.

From the four cyclic local minima of the potential energy surface, the most stable one is again cycle **A**. This structure is followed in stability by another cyclic structure, **B**, that, as with the previous one, can be seen as the result of the interaction of a MgH_2 monomer with the $\text{MgH}_2\text{-MgH}_2$ dimer. Cycles **A** and **B** are distinguished by the *cis* or *trans* arrangement of hydrogens 6 and 9 in the dimer, with the result that in **B**, the 1Mg atom is only tricoordinated. At this point, it should be noted, as mentioned previously, that for the BeH_2 trimers, only **A** was found to be stable, as any attempt to find **B** led to the linear trimer.

The third cyclic isomer in terms of stability is a planar hexagonal structure, though another non-planar conformer (not shown in Figure 4) was found to be also a local minimum, but $7 \text{ kJ}\cdot\text{mol}^{-1}$ less stable. The bonding analysis discussed above for the BeH_2 trimers (linear and **A**) can be extended to the MgH_2 ones, and for similar reasons, again, the linear tautomer is slightly more stable than the trimer **A**. Specifically, the linear MgMgMgH_6 trimer is $20 \text{ kJ}\cdot\text{mol}^{-1}$ less stable than its Be-containing analogue. For this structure, in line with what was discussed for the dimers, the Δ^2E attractive interactions and the E_R repulsive ones are smaller in MgMgMgH_6 than in the BeBeBeH_6 analog (see Table 2), resulting in a smaller stabilizing enthalpy in the former. A comparison of Figures 3 and 4 shows that the structure of cluster **A** for Mg is less compact than the homologous Be-containing isomer due to the longer interatomic distances (see Table S4 of the Supplementary Materials). Consistently, some of the non-covalent interactions are weaker. NCIPLOT shows that, due to its smaller compactness, the attractive homogeneous interstitial density between the Mg atoms and the hydrogens is less strongly attractive than in the Be analog. Going from cluster **A** to **B**, as expected, the overall attractive contributions (Δ^2E and Δ^3E) decrease by about $6 \text{ kJ}\cdot\text{mol}^{-1}$, whereas the E_R terms increase by about the same amount, explaining why complex **B** is only $12 \text{ kJ}\cdot\text{mol}^{-1}$ less stable than conformer **A**. The lower stability of the hexagonal cycle just reflects the decrease in the Δ^2E attractive terms because no 3c-2e bonds are formed in this case, which is only partially compensated by an increase of the Δ^3E contribution due to the hexagonal arrangement of this complex.

The stability trends of the different conformers change dramatically when moving to the halides, though the linear trimer is still the global minimum. Let us discuss the fluorides shown in Figure 5 in more detail.

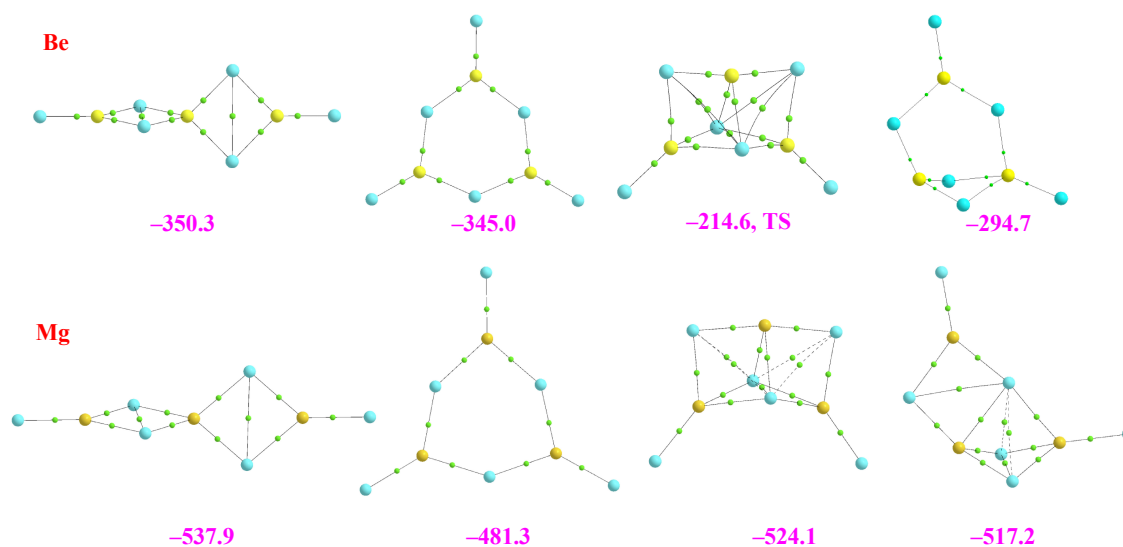


Figure 5. Molecular graphs of the homotrimers involving BeF_2 and MgF_2 . The numbers in magenta are the stabilization enthalpies in $\text{kJ}\cdot\text{mol}^{-1}$.

For the BeF_2 trimers, the linear arrangement is the global minimum, followed by the hexagonal cycle, only $5 \text{ kJ}\cdot\text{mol}^{-1}$ less stable, and by cycle **B**, which is $50 \text{ kJ}\cdot\text{mol}^{-1}$ further less stable. In this case, cycle **A** is a stationary point with one imaginary frequency. The same clusters are found when Be is replaced by Mg, but in this case, all of them are local minima of the potential energy surface. However, the energy trends are totally different, with cycle **A** being the second most stable after the linear trimer. As in the dimers, the dominant electrostatic character in fluorides renders the linear trimer more stable than the homologous containing BeH_2 (-350.3 vs. $-301.3 \text{ kJ}\cdot\text{mol}^{-1}$). Conversely, since this dominant electrostatic character prevents the formation of 3c-2e bonds, cycle **A** is found to be significantly less stable than its homologous hydride (-214.6 vs. $-277.1 \text{ kJ}\cdot\text{mol}^{-1}$). Cycle **A** is indeed much less stable than the linear trimer due to its compactness, which

results in a close vicinity of F atoms reflected by the repulsive terms in the LMO-EDA results of Table S5. The consequence is that for the fluorides, **A** is a TS that leads to the linear cluster. The MBIE analysis (see Table 2) also shows that the hexagonal cycle is marginally less stable than the linear trimer. This is caused by the very small difference between the attractive ($\Delta^2E + \Delta^3E$) and the repulsive (E_R) terms, which is slightly greater ($4 \text{ kJ}\cdot\text{mol}^{-1}$) than in the former, so those species can be considered practically degenerate. The main difference when dealing with the Mg-containing systems is the larger size of Mg and the much longer bonds, which contribute to significantly stabilizing cycles **A** and **B**. These cycles are less compact, closing the gap with respect to the linear global minimum. It should be mentioned that although the MgF_2 trimers we found coincide with those in the literature [25], this is not the case as far as their stabilization energies are concerned since our G4 and M06-2X calculations both predict a different stability order (see Table S6 of the Supplementary Materials), likely due to the effect of dispersion contributions only included in our calculations.

The structures and stabilities of the homotrimer chlorides are presented in Figure S4 of the Supplementary Materials. As was the case for the hydrides and fluorides, the most stable trimer is the linear one. However, there are some differences with respect to fluorides in what concerns the relative stabilities of the other minima. For BeF_2 homotrimers, the hexagonal trimer is planar, whereas in the corresponding chloride, it is not. On top of that, the fluoride is $5 \text{ kJ}\cdot\text{mol}^{-1}$ less stable than the linear conformer, whereas for the chloride, this gap becomes ten times larger. Also, for Be trimers, cycle **A** is found to be a TS and the least stable stationary point, showing once more the significative effect of the repulsion in these compact systems when the substituent is voluminous as Cl. Conversely, for Mg, where these interactions are much weaker due to the much larger interatomic distances (see Table S4 of the Supplementary Materials), cycle **A** is not only a minimum but close in energy to the global minimum.

2.3. Heterotrimers

The conformational richness when dealing with heterotrimers is very high. Starting from the linear clusters, the number multiplies by three on going from homo to heterodimers. This can be easily understood if we remember that a linear trimer can be seen as the result of the interaction of a dimer with a monomer along the axis. Hence, if we take the homodimers $\text{X}_2\text{Be}-\text{BeX}_2$, its interaction can be exclusively with MgX_2 , leading to a unique $\text{BeX}_2\text{BeX}_2\text{MgX}_2$ arrangement. However, if the interaction involves the heterodimer, $\text{X}_2\text{Be}-\text{MgX}_2$, the interaction can take place with any of the two monomers. The interaction with BeX_2 will yield the same trimer as before if the attachment takes place on the BeX_2 or to a new $\text{BeX}_2\text{MgX}_2\text{BeX}_2$ conformer if this attachment takes place on the MgX_2 side. If the monomer involved is MgX_2 , two new clusters, $\text{MgX}_2\text{BeX}_2\text{MgX}_2$ and $\text{BeX}_2\text{BeX}_2\text{MgX}_2$, would be produced. All these possibilities, with their corresponding stabilization enthalpies, are shown in Figure 6. As expected from our discussion on the dimers, fluorides are significantly more stable than hydrides, whereas chlorides are only slightly more stable or unstable than hydrides, depending on the case. A second conspicuous fact is that this stability depends on the nature of the central atom and that the stabilities observed for the hydrides reverse on going to fluorides and chlorides. Indeed, for the hydrides, the most stable linear clusters of each kind are those in which the central atom is Be, whereas in fluorides and chlorides, the most stable are systematically those in which the central atom is Mg.

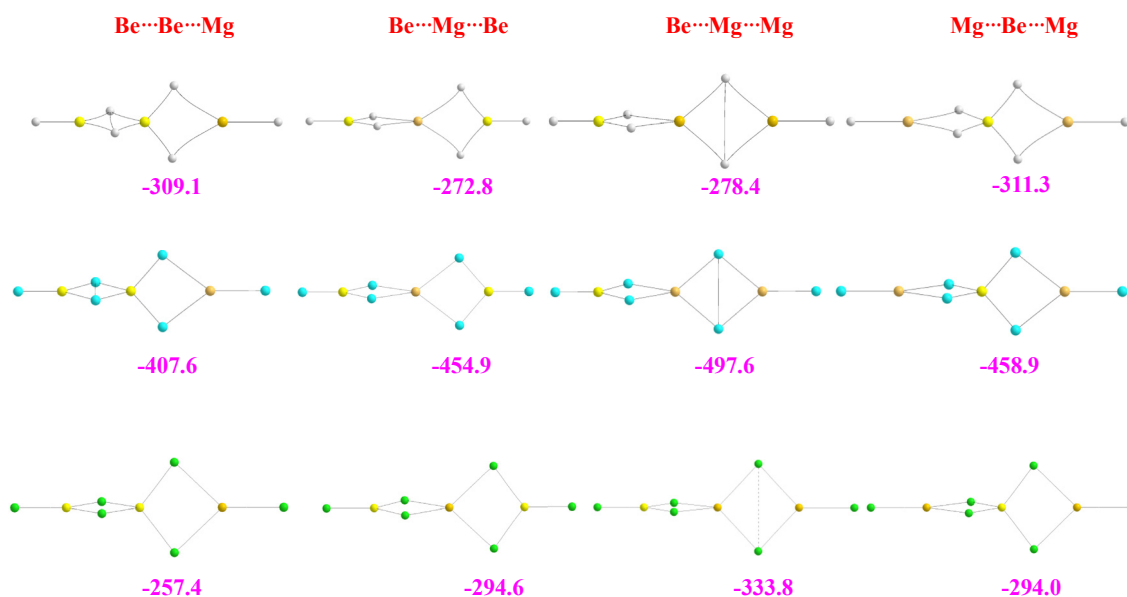


Figure 6. Molecular graphs for the linear heterotrimers, showing their stabilization enthalpies in $\text{kJ}\cdot\text{mol}^{-1}$.

This finding is the result of mainly two features: the distortion energies of the central atom and the three-body contributions to the total energy. As it can be seen in Table S7 of the Supplementary Materials, for the hydrides, E_R is almost twice when the central atom is Be instead of Mg. This effect is more than compensated by the $\Delta^2 E$ terms, more negative in the first case, but mainly by the $\Delta^3 E$ term, more than three times larger in the former than in the latter thanks to stronger 3c-2e bonds in $\text{H}_2\text{Be}-\text{BeH}_2$ than in $\text{BeH}_2-\text{MgH}_2$. When moving to the halides, the $\Delta^3 E$ contribution is marginal because, in these systems, no 3c-2e bonds are formed. It only remains, as a key factor, the much higher E_R value when the central atom is Be, leading to less stable clusters than those where the central atom is Mg.

Concerning the cyclic trimers, one option is the formation of hexagonal trimers, also found for the homotrimers. However, these structures were only found to be stable for hydrides and fluorides, but in both cases, more than $50 \text{ kJ}\cdot\text{mol}^{-1}$ is less stable than the corresponding linear trimers (see Figure S5 of the Supplementary Materials). More interesting are the cycles similar to the clusters **A** and **B** described in the homotrimers section. When dealing with heterotrimers, the different cycles that can be envisaged amount to five instead of two, as shown in Figure 7.

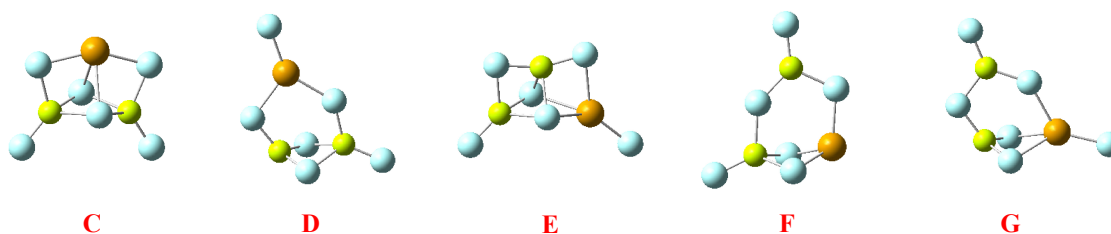
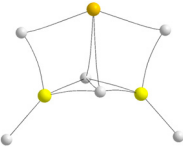
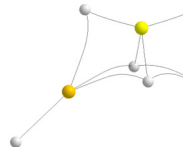
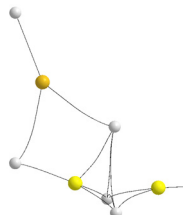
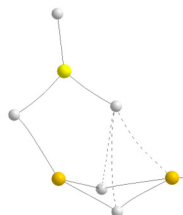
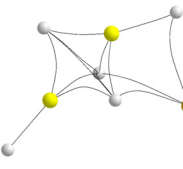
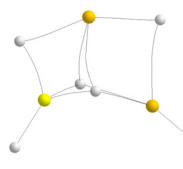
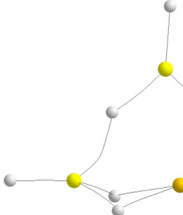
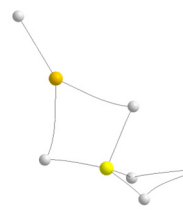


Figure 7. Different kinds of cyclic heterotrimers formed by the interaction of a dimer with a monomer that approaches the former in a direction perpendicular to the dimer axis.

Cycles **C** and **D** result from the interaction of a homodimer with a different monomer. They differ in the *cis* (**C**) or *trans* (**D**) arrangement of the terminal substituents of the homodimer. On the other hand, cycles **E**, **F**, and **G** arise from the interaction between a heterodimer and a certain monomer. Again, if the substituents of the dimer are *cis*, cycle **E** is formed. If the substituents are *trans*, there are two possibilities, cycles **F** and **G**. The important matter is that in some specific cases, these cycles become the global minimum of

the potential energy surface. Let us start with the hydrides. The molecular graphs of these clusters are shown in Table 3, together with their stabilization enthalpies and their relative enthalpies with respect to the corresponding linear trimers in Figure 6.

Table 3. Molecular graphs of cycles C–G of $\text{BeH}_2\text{BH}_2\text{MgH}_2$ and $\text{BeH}_2\text{MgH}_2\text{MgH}_2$ and their stabilization enthalpies (bold numbers). In blue, their relative stabilities with respect to the corresponding linear trimer are also provided. In red, the two cases in which the cycle is the global minimum. All values in $\text{kJ}\cdot\text{mol}^{-1}$.

	BeBeMgH₆		BeMgMgH₆	
	Molecular graph	Stab. enth./ Rel. Stab.	Molecular graph	Stab. enth./ Rel. Stab.
<i>Trimers</i>	BeBeMg		BeMgMg	
C		−253.6 55.5		−319.5 −8.2
D		−299.8 9.3		−248.4 62.9
E		−313.7 −4.6		−271.3 40.0
F		−221.7 87.4		−208.1 103.2

The first conspicuous fact is that cycle **G** does not exist because it collapses to the linear global minimum. The second and most important is that some of them are rather stable, to the point that one within each family is predicted to be the global minimum of the potential energy surface (negative relative stabilities in red). This is a result of subtle differences, related again essentially to the distortion energy of the monomers and the Δ^3E terms. In cycle **E** (see Table S8 of the Supplementary Materials), the E_R contributions are smaller than in the linear trimer because the BeH_2 moiety at the top of the cycle is almost linear. As expected, the three Δ^2E in cycle **E** are negative, whereas in the linear trimer, only those of the central unit with the other two are negative. The overall balance is still favorable to the linear trimer, but this is compensated by a larger Δ^3E contribution, which renders cycle **E** the most stable. For the case of the BeMgMgH_6 heterotrimers, the situation is slightly different. Now, the E_R contributions are very similar in both cycle **C** and the linear trimer (see Table S8 of the Supplementary Materials) because of a larger distortion of the Be derivative at the top in cycle **C**. Since the Δ^2E contributions are globally similar,

even though in the linear trimer, as expected, only two are significantly large, the enhanced stability of cycle **C** comes essentially from the Δ^3E term. Hence, once more, the two key factors are the E_R and the Δ^3E components, and when the former does not contribute significantly, it is only the Δ^3E term that is behind the stability differences.

When moving to fluorides and chlorides, the scenario changes completely with respect to the relative stability of cycles **C–G** (see Table S9 of the Supplementary Materials). Indeed, neither in the fluorides nor in the chlorides do the cyclic trimers compete in stability with the linear ones. This reflects the fact already mentioned in previous sections: the dominant electrostatic character of the interactions avoids the formation of 3c-2e bonds and, accordingly, since these cycles are rather compact structures, the repulsive interactions between the substituents increase significantly, and the Δ^3E contributions become highly unstabilizing (see Table S10 of the Supplementary Materials).

3. Computational Details

The first step of our analysis was a screening of the different dimers and trimers that can be possible minima of the corresponding potential energy surface. From them, we chose the most stable form for each of the different isomers, linear or cyclic. It should be mentioned that for the particular cases of BeH_2 , MgH_2 , MgF_2 , and MgCl_2 trimers, our most stable structures are the same as those previously reported in the literature [10,24–26].

The structure and final energies of the clusters under investigation were obtained using both *ab initio* and density functional theory methods. In the first case, we have used the composite Gaussian-4 (G4) formalism [29]. In this method, the different *ab initio* calculations are carried out on geometries optimized with the B3LYP DFT approach together with a 6-31G(2df,p) basis set expansion. Final energies are calculated by combining different methods that properly account for the electron correlation effects, namely Møller–Plesset (MPn) perturbation theory up to the fourth order and CCSD(T) coupled-cluster theory. A final correction should be added to this: an estimation of the Hartree–Fock energy limit (HF limit) together with two high-level empirical corrections. The result is that final energies are accurate up to a CCSD(T,full)/G3LargeXP + HF limit level, with an average absolute deviation [29] of $3.47 \text{ kJ}\cdot\text{mol}^{-1}$.

For our DFT calculations, we have chosen the B3LYP method, which is the one used in the G4 formalism for the geometry optimizations. To specifically check whether dispersion effects are significant for the systems under investigation, we have also added to the B3LYP method the D3BJ empirical dispersion term proposed by Grimme, including the Becke–Johnson damping correction [30]. The second DFT method chosen was the M06-2X, as this functional also provides much better quality descriptions of dispersion-dominated systems than standard functionals [31]. Moreover, M06-2X yields values that correlate very well with the MP2 ones, in particular when an extended basis set is used [32–35]. Very recently, we have found it to provide results in good agreement with G4 calculations when dealing with clusters involving electron-deficient systems [7]. For all these DFT calculations, a rather flexible aug-cc-pVTZ basis set has been used.

In particular, when dealing with trimers, a good understanding of the nature of bonds in this kind of cluster requires knowing the contribution of one-, two- and three-body terms, as well as the weight of the electrostatic, exchange, and dispersion contributions to the total binding energy.

For the first goal, we have used the many-body interaction energy (MBIE) formalism [36,37], which, for a ternary complex, allows the decomposition of the total binding energy ΔE (Equation (1)) into one- (Equation (2)), two- (Equation (3)), and three-body interactions (Equation (4)), as follows:

$$\Delta E = E(ABC) - \sum_{i=A}^C E_m(i) = \sum_{i=A}^C E_R(i) + \sum_{i=A}^B \sum_{j>i}^C \Delta^2 E(i, j) + \Delta^3 E(ABC) \quad (1)$$

$$E_R(i) = E(i) - E_m(i) \quad (2)$$

$$\Delta^2 E(ij) = E(ij) - [E(i) + E(j)] \quad (3)$$

$$\Delta^3 E(ABC) = E(ABC) - [E(A) + E(B) + E(C)] - [\Delta^2 E(AB) + \Delta^2 E(AC) + \Delta^2 E(BC)] \quad (4)$$

The value of $E_R(i)$, which measures the energy associated with the monomer distortion when it is part of the trimer, is the difference between $E_m(i)$, the energy of the *i*-monomer in its equilibrium geometry, and $E(i)$, the energy of the *i*-monomer within the geometry of the ABC complex. $\Delta^2 E(ij)$ and $\Delta^3 E(ABC)$ are the two- and three-body interaction energies computed at the corresponding geometries in the complex. For the second objective, we have employed the LMO-EDA [38] decomposition analysis based on the generalized Kohn–Sham (GKS) and localized molecular orbitals, which permits us to write the total interaction energy as the sum of electrostatic, exchange, repulsion, polarization, and dispersion contributions (Equation (5)).

$$E_{\text{int}} = E_{\text{elec}} + E_{\text{exc}} + E_{\text{rep}} + E_{\text{pol}} + E_{\text{disp}} \quad (5)$$

It should be mentioned that the distortion energy present in the MBIE analysis is not included in the LMO-EDA energy decomposition procedure. The LMO-EDA calculations were carried out by using the GAMESS code (version 2012-R1) [39].

To detect the new bonds that stabilize each cluster and to have reliable information on their nature and strength, we have carried out a topological analysis of the molecular electron density, $\rho(r)$, by means of the Atoms in Molecules (AIM) approach [40], using the AIMAll (Version 19.10.12) code [41]. In this way, we could locate its first-order saddle points, the so-called bond critical points (BCPs), and obtain the corresponding molecular paths that provide information on the bonds stabilizing the system. In fact, since an inspection of the cluster structures in terms of interatomic distances and angles does not necessarily lead to knowing which bonds have been formed, the discussion of the cluster structures will be carried out using the corresponding molecular graphs. In all cases, the AIM analysis was followed by NBO (Natural Bond Orbitals) [42] calculations to complement the bonding information, in particular on what concerns the formation of (3c-2e) bonds. These calculations have been carried out with the NBO 5.G code [43]. In this respect, another useful technique to detect the existence of multicenter bonds is the AdNDP analysis [44], which was used for dimers and trimers. For those systems in which non-covalent interactions might be present, the information provided by the AIM method is nicely complemented by the NCIPLOT approach [45], which allows finding regions of low reduced density gradient (*s*) and low-density values typically associated with these non-covalent interactions.

Further information on the bonding of these clusters may be obtained by using the Electron Localization Function (ELF) formalism [46], which permits the location of the areas in which the electrons of the system are distributed in monosynaptic and disynaptic (or polysynaptic) basins. These regions are characterized by a low value of the excess local kinetic energy, thus identifying highly localized electrons. Monosynaptic basins are typically associated with core and electron lone pairs, whereas disynaptic (or polysynaptic) basins are associated with two-center (or more than two) bonding interactions.

4. Conclusions

Considering the unpaired electron available for bonding in H and halogens, one might expect that clustering between pure and mixed beryllium and magnesium clusters could follow relatively similar stabilities and bonding patterns for these substituents. However, a global picture of the dimers and trimers of this family offers a much more complex panorama. This work has dealt with the reasons behind the observed trends.

We have seen that magnesium homodimers are significantly more stable than beryllium homodimers and heterodimers and that the largest stabilization enthalpies are those of the fluorides, far from hydrides and chlorides, which are more alike. Thanks to LMO-EDA

and NBO/AdNDP, we have shown that the electrostatic component is, as expected, much larger in halides than in hydrides, but chlorine has a lower contribution because of its larger size and cannot form multicenter two-electron bonds as hydrides do. The MBIE analysis helped to reveal the importance of the deformation (rehybridization) energy cost, which is much larger for beryllium than for magnesium.

Regarding the hydride homotrimers, we have understood why cyclic structures such as cyclic **A** can compete in stability with the linear structure. As the MBIE showed, in line with observations through topological tools, not only the strength of binding interactions must be taken into account but also the distortion involved to form the structures, together with the presence of non-covalent interactions in cycle **A** that have to be properly included in the theoretical treatment. Instead, beryllium fluoride clusters prefer the linear conformation, avoiding the compactness of cyclic structures, whereas magnesium, with larger bonds, presents cyclic structures **A** and **B** closer in energy to the linear one.

Finally, we have also paid attention to hydride heterotrimers, locating linear and several cyclic structures, where the many-body interactions allowed us to explain the preferences for central Be or Mg atoms in the linear structures. MBIE can also rationalize the subtle differences in the cyclic cases and explain why, for the BeBeMgH₆ and BeMgMgH₆ hydrides, the compact cycles, as **C** and **E**, become the global minima, respectively. However, halogen heterotrimers cannot compete in their cyclic forms with the linear ones in the absence of multicenter two-electron bonds and the predominance of three-body unstabilizing terms. As a final comment, we would like to point out that the study of the interactions between the BeCl₂ dimers with phosphorus-containing compounds reported in ref. [23] suggests that the clusters investigated here may exhibit a rather interesting reactivity, whose study could be a good benchmark to analyze it in terms of HOMO-LUMO interactions, as proposed in a very recent publication [47].

Supplementary Materials: The following supporting information can be downloaded at: <https://www.mdpi.com/article/10.3390/molecules28227507/s1>. Figure S1. Correlation between G4 and M06-2X interaction enthalpies. Figure S2. Correlation between the interaction enthalpies calculated at the G4 and B3LYP levels of theory. Table S1. LMO-EDA analysis for BeBeX₄, MgMgX₄ and BeMgX₄ (X = H, F, Cl) dimers. Figure S3. Molecular graphs of the homo and heterodimers involving BeX₂ and MgX₂ (X = H, F, Cl) monomers, showing the electron density, its Laplacian and the energy density at the bond critical points (BCPs). Table S2. AdNDP orbital list for the BeBeX₄, MgMgX₄ and BeMgX₄ dimers. Table S3. Wiberg bond indexes for Be₂X₄, Mg₂X₄, BeMgX₄ (X = H, F, Cl). Table S4. Interatomic distances in the cycles **A** of Be₂H₄ and Mg₂H₄. Table S5. LMO-EDA analysis for the BeBeBeF₆ trimers. Figure S4. Bond paths and stabilization enthalpies for the BeCl₂ and MgCl₂ homotrimers. Table S6. Relative stabilities for the MgF₂ trimers obtained by different theoretical approaches. Table S7. MBIE analysis of linear heterotrimer complexes formed by BeX₂ and MgX₂ (X = H, F, Cl). Figure S5. Bond paths for the stable hexagonal heterotrimers BeCl₂ and MgCl₂ homotrimers, showing their stabilization and relative enthalpies with respect to the corresponding linear heterotrimer in kJ·mol⁻¹. Table S8. MBIE analysis of BeBeMgH₆ and BeMgMgH₆ heterotrimer complexes. Table S9. Molecular graphs of cycles **C-G** of BeX₂BX₂MgX₂ and BeX₂MgX₂MgX₂ (X = F, Cl) and their stabilization enthalpies. Table S10. MBIE analysis of heterotrimer complexes for fluorides and chlorides.

Author Contributions: Conceptualization, I.A., M.M.M.-C., J.E., O.M. and M.Y.; methodology, I.A., M.M.M.-C. and M.Y.; software, I.A. and M.M.M.-C.; validation, I.A., M.M.M.-C. and M.Y.; formal analysis, I.A., M.M.M.-C., J.E., O.M. and M.Y.; investigation, I.A., M.M.M.-C., J.E., O.M. and M.Y.; resources, I.A. and M.Y.; writing—original draft preparation, M.Y.; writing—review and editing, I.A., M.M.M.-C., J.E., O.M. and M.Y.; visualization, I.A., M.M.M.-C., J.E., O.M. and M.Y.; supervision, I.A., M.M.M.-C., J.E., O.M. and M.Y.; project administration, I.A. and M.Y.; funding acquisition, I.A., M.Y. and O.M. All authors have read and agreed to the published version of the manuscript.

Funding: This research was funded by Projects PID2021-125207NB-C31, PID2021-125207NB-C32, and PID2019-110091GB-I00 from the Ministerio de Ciencia e Innovación (MICINN) of Spain.

Institutional Review Board Statement: Not applicable.

Informed Consent Statement: Not applicable.

Data Availability Statement: The authors confirm that the data supporting the findings of this study are available within the article and its Supplementary Materials.

Acknowledgments: We acknowledge the help provided by Al Mokhtar Lamsabhi to carry out the screening of possible conformers. Computational time at Centro de Computación Científica (CCC) of Universidad Autónoma de Madrid is also acknowledged.

Conflicts of Interest: The authors declare no conflict of interest.

References and Note

1. Lipscomb, W.N. Advances in Theoretical Studies of Boron Hydrides and Carboranes. In *Boron Hydride Chemistry*; Muetterties, E.L., Ed.; Academic Press: Itaca, NY, USA, 1975; pp. 39–78.
2. Mayer, I. Bond orders in 3-center bonds—An analytical investigation into the electronic-structure of diborane and the 3-center 4-electron bonds of hypervalent sulfur. *J. Mol. Struct. Theochem* **1989**, *55*, 43–52. [\[CrossRef\]](#)
3. Liang, C.X.; Davy, R.D.; Schaefer, H.F. Infrared-spectra of the unknown dialane (Al_2H_6) and recently observed digallane (Ga_2H_6) molecules. *Chem. Phys. Lett.* **1989**, *159*, 393–398. [\[CrossRef\]](#)
4. Lammertsma, K.; Leszczynski, J. Ab initio study on dialane(6) and digallane(6). *J. Phys. Chem.* **1990**, *94*, 2806–2809. [\[CrossRef\]](#)
5. Andrews, L.; Wang, X.F. The infrared spectrum of Al_2H_6 in solid hydrogen. *Science* **2003**, *299*, 2049–2052. [\[CrossRef\]](#)
6. Nori-Shargh, D.; Yahyaei, H.; Mousavi, S.N.; Maasoomi, A.; Kayi, H. Natural bond orbital, nuclear magnetic resonance analysis and hybrid-density functional theory study of sigma-aromaticity in Al_2F_6 , Al_2Cl_6 , Al_2Br_6 and Al_2I_6 . *J. Mol. Model.* **2013**, *19*, 2549–2557. [\[CrossRef\]](#) [\[PubMed\]](#)
7. Mó, O.; Montero-Campillo, M.M.; Yáñez, M.; Alkorta, I.; Elguero, J. Dispersion, Rehybridization, and Pentacoordination: Keys to Understand Clustering of Boron and Aluminum Hydrides and Halides. *J. Phys. Chem. A* **2023**, *127*, 5860–5871. [\[CrossRef\]](#)
8. Ahlrichs, R. Ab initio Calculations on Small Hydrides Including Electron Correlation. *Theoret. Chim. Acta* **1970**, *17*, 348–361. [\[CrossRef\]](#)
9. Kirillov, Y.B.; Boldyrev, A.I.; Klimenko, N.M.; Charkin, O.P. An ab initio calculation of the structure and stability of the complex hydrides MgBeH - and Mg_2H -. *J. Struct. Chem.* **1983**, *24*, 134–136. [\[CrossRef\]](#)
10. Chen, Y.L.; Huang, C.H.; Hu, W.P. Theoretical study on the small clusters of LiH , NaH , BeH_2 , and MgH_2 . *J. Phys. Chem. A* **2005**, *109*, 9627–9636. [\[CrossRef\]](#) [\[PubMed\]](#)
11. Lingam, C.B.; Babu, K.R.; Tewari, S.P.; Vaitheeswaran, G. Quantum chemical studies on beryllium hydride oligomers. *Comput. Theor. Chem.* **2011**, *963*, 371–377. [\[CrossRef\]](#)
12. Alkorta, I.; Elguero, J.; Solimannejad, M.; Grabowski, S.J. Dihydrogen Bonding vs. Metal- σ Interaction in Complexes between H_2 and Metal Hydride. *J. Phys. Chem. A* **2011**, *115*, 201–210. [\[CrossRef\]](#)
13. Erfort, S.; Tschope, M.; Rauhut, G. Efficient and automated quantum chemical calculation of rovibrational nonresonant Raman spectra. *J. Chem. Phys.* **2022**, *156*, 124102. [\[CrossRef\]](#)
14. Erfort, S.; Tschope, M.; Rauhut, G. Toward a fully automated calculation of rovibrational infrared intensities for semi-rigid polyatomic molecules. *J. Chem. Phys.* **2020**, *152*, 244104. [\[CrossRef\]](#) [\[PubMed\]](#)
15. Wang, X.F.; Andrews, L. Infrared spectra of magnesium hydride molecules, complexes, and solid magnesium dihydride. *J. Phys. Chem. A* **2004**, *108*, 11511–11520. [\[CrossRef\]](#)
16. Abdurahman, A. Ab initio studies of static dipole polarizability of the polymeric beryllium hydride chain. *J. Phys. Chem. A* **2003**, *107*, 11547–11552. [\[CrossRef\]](#)
17. Wang, X.F.; Andrews, L. One-dimensional BeH_2 polymers: Infrared spectra and theoretical calculations. *Inorg. Chem.* **2005**, *44*, 610–614. [\[CrossRef\]](#)
18. Ramondo, F.; Bencivenni, L.; Spoliti, M. Ab initio study on the Be_2F_4 , Mg_2F_4 dimers, on the mixed dimers BeMgF_4 and LiNaF_2 and on the Li_2BeF_4 , LiBeCl_4 and LiAlCl_4 ion-pairs. *J. Mol. Struct. Theochem* **1992**, *96*, 171–184. [\[CrossRef\]](#)
19. Gigli, G. On the structure of the alkaline earth dihalides dimers. *J. Chem. Phys.* **1990**, *93*, 5224–5233. [\[CrossRef\]](#)
20. Ystenes, B.K. Quantum chemical studies of molecular difluorides and dichlorides of beryllium and magnesium. *Spectrochim. Acta A Mol. Biomol. Spectrosc.* **1998**, *54*, 855–868. [\[CrossRef\]](#)
21. Molnar, J.; Marsden, C.J.; Hargittai, M. Molecular-structures and force-fields of monomeric and dimeric magnesium dichloride from electron-diffraction and quantum-chemical calculations. *J. Phys. Chem.* **1995**, *99*, 9062–9071. [\[CrossRef\]](#)
22. Girichev, A.G.; Giricheva, N.I.; Vogt, N.; Girichev, G.V.; Vogt, J. Structural investigation of molecules in the vapour over beryllium dichloride using electron diffraction and mass spectrometric data. *J. Mol. Struct.* **1996**, *384*, 175–182. [\[CrossRef\]](#)
23. Buchner, M.R.; Spang, N.; Ivlev, S.I. Hydrolysis and oxidation products of phosphine adducts to beryllium chloride. *Z. Naturforsch. B J. Chem. Sci.* **2022**, *77*, 381–390. [\[CrossRef\]](#)
24. Eichkorn, K.; Schneider, U.; Ahlrichs, R. An ab-initio investigation of structure and energetics of clusters $\text{Mg}_n\text{Cl}_{2n}$. *J. Chem. Phys.* **1995**, *102*, 7557–7563. [\[CrossRef\]](#)
25. Neogi, S.G.; Chaudhury, P. Structure, electronic properties and vibrational spectra of $(\text{MgF}_2)_n$ clusters through a combination of genetic algorithm and DFT-based approach. *Mol. Phys.* **2015**, *113*, 3729–3739. [\[CrossRef\]](#)

26. Luhtanen, T.N.P.; Linnolahti, M.; Laine, A.; Pakkanen, T.A. Structural characteristics of small magnesium dichloride clusters: A systematic theoretical study. *J. Phys. Chem. B* **2004**, *108*, 3989–3995. [\[CrossRef\]](#)
27. Values calculated at the M06-2X/aug-cc-pVTZ level of theory (this work).
28. Wiberg, K.B. Application of pople-santry-segal cndo method to cyclopropylcarbinyl and cyclobutyl cation and to bicyclobutane. *Tetrahedron* **1968**, *24*, 1083–1088. [\[CrossRef\]](#)
29. Curtiss, L.A.; Redfern, P.C.; Raghavachari, K. Gaussian-4 theory. *J. Chem. Phys.* **2007**, *126*, 084108. [\[CrossRef\]](#)
30. Grimme, S.; Ehrlich, S.; Goerigk, L. Effect of the Damping Function in Dispersion Corrected Density Functional Theory. *J. Comp. Chem.* **2011**, *32*, 1456–1465. [\[CrossRef\]](#)
31. Grimme, S.; Hansen, A.; Brandenburg, J.G.; Bannwarth, C. Dispersion-Corrected Mean-Field Electronic Structure Methods. *Chem. Rev.* **2016**, *116*, 5105–5154. [\[CrossRef\]](#)
32. Walker, M.; Harvey, A.J.A.; Sen, A.; Dessent, C.E.H. Performance of M06, M06-2X, and M06-HF Density Functionals for Conformationally Flexible Anionic Clusters: M06 Functionals Perform Better than B3LYP for a Model System with Dispersion and Ionic Hydrogen-Bonding Interactions. *J. Phys. Chem. A* **2013**, *117*, 12590–12600. [\[CrossRef\]](#)
33. Castro-Alvarez, A.; Cameros, H.; Sanchez, D.; Vilarrasa, J. Importance of the Electron Correlation and Dispersion Corrections in Calculations Involving Enamines, Hemiaminals, and Amins. Comparison of B3LYP, M06-2X, MP2, and CCSD Results with Experimental Data. *J. Org. Chem.* **2015**, *80*, 11977–11985. [\[CrossRef\]](#) [\[PubMed\]](#)
34. Lopez-Lopez, J.A.; Ayala, R. Assessment of the performance of commonly used DFT functionals vs. MP2 in the study of IL-Water, IL-Ethanol and IL-(H₂O)(3) clusters. *J. Mol. Liq.* **2016**, *220*, 970–982. [\[CrossRef\]](#)
35. Stortz, C.A.; Sarotti, A.M. Exhaustive exploration of the conformational landscape of mono- and disubstituted five-membered rings by DFT and MP2 calculations. *RSC Adv.* **2019**, *9*, 24134–24145. [\[CrossRef\]](#)
36. Hankins, D.; Moskowitz, J.W.; Stillinger, F.H. Water molecule interactions. *J. Chem. Phys.* **1970**, *53*, 4544–4554. [\[CrossRef\]](#)
37. Xantheas, S.S. Ab-initio studies of cyclic water clusters (H₂O)_n, n=1-6. 2. Analysis of many-body interactions. *J. Chem. Phys.* **1994**, *100*, 7523–7534. [\[CrossRef\]](#)
38. Su, P.F.; Jiang, Z.; Chen, Z.C.; Wu, W. Energy Decomposition Scheme Based on the Generalized Kohn-Sham Scheme. *J. Phys. Chem. A* **2014**, *118*, 2531–2542. [\[CrossRef\]](#)
39. Schmidt, M.W.; Baldridge, K.K.; Boatz, J.A.; Elbert, S.T.; Gordon, M.S.; Jensen, J.H.; Koseki, S.; Matsunaga, N.; Nguyen, K.A.; Su, S.J.; et al. General atomic and molecular electronic-structure system. *J. Comp. Chem.* **1993**, *14*, 1347–1363. [\[CrossRef\]](#)
40. Bader, R.F.W. *Atoms in Molecules. A Quantum Theory*; Clarendon Press: Oxford, UK, 1990; pp. 1–456.
41. Keith, T.A. AIMAll, version 19.10.12; TK Gristmill Software: Overland Parks, KS, USA, 2019. Available online: aim.tkgristmill.com (accessed on 1 January 2023).
42. Reed, A.E.; Weinhold, F. Natural localized molecular-orbitals. *J. Chem. Phys.* **1985**, *83*, 1736–1740. [\[CrossRef\]](#)
43. Glendening, E.D.; Badenhoop, J.K.; Reed, A.E.; Carpenter, J.E.; Bohmann, J.A.; Morales, C.M.; Weinhold, F. NBO 5.G; Theoretical Chemistry Institute, University of Wisconsin: Madison, WI, USA, 2004.
44. Tkachenko, N.V.; Boldyrev, A.I. Chemical bonding analysis of excited states using the adaptive natural density partitioning method. *Phys. Chem. Chem. Phys.* **2019**, *21*, 9590–9596. [\[CrossRef\]](#) [\[PubMed\]](#)
45. Boto, R.A.; Peccati, F.; Laplaza, R.; Quan, C.; Carbone, A.; Piquemal, J.P.; Maday, Y.; Contreras-García, J. NCIPLLOT4: Fast, robust and quantitative analysis of non-covalent interactions. *J. Chem. Theory Comp.* **2020**, *16*, 4150–4158. [\[CrossRef\]](#) [\[PubMed\]](#)
46. Savin, A.; Nesper, R.; Wengert, S.; Fässler, T.F. ELF: The electron localization function. *Angew. Chem. Int. Edit.* **1997**, *36*, 1809–1832. [\[CrossRef\]](#)
47. Santos, L.D.; Ramalho, T.C.; Hamlin, T.A.; Bickelhaupt, F.M. Intermolecular Covalent Interactions: Nature and Directionality. *Chem. Eur. J.* **2023**, *29*, e202203791. [\[CrossRef\]](#) [\[PubMed\]](#)

Disclaimer/Publisher's Note: The statements, opinions and data contained in all publications are solely those of the individual author(s) and contributor(s) and not of MDPI and/or the editor(s). MDPI and/or the editor(s) disclaim responsibility for any injury to people or property resulting from any ideas, methods, instructions or products referred to in the content.